Blade Loading and Rotation Effects on Compressor Rotor Wake Near End Walls

B. Lakshminarayana,* T. R. Govindan,† and B. Reynolds‡
The Pennsylvania State University, University Park, Pennsylvania

This study was carried out to understand the effects of blade loading and rotation on the rotor end wall flow structure, including the wake. The measurements were taken with a stationary three sensor hot wire located at the exit of a compressor rotor. The signal was ensemble averaged to derive all the three components of velocity and six components of stresses at the exit. Measurements were made at two different rotational speeds (1753 and 1010 rpm) but the same loading, and at two differing blade loadings (1753 and 1499 rpm) at several radii near the hub and the annulus wall. The wake decay in the annulus wall region is found to be much more rapid than the midspan regions. Furthermore, both the loading and rotation of the blade have appreciable influence on the end wall flow and wake structure. Interaction of the annulus and hub wall boundary layers (and secondary flow resulting from these) have appreciable influence on the wake structure in the end wall regions.

Nomenclature

C = chord length
i = incidence
L_p, L_s = wake width at half the depth on the pressure and suction sides of the wake, respectively, based on axial velocity profiles
N = speed, rpm
Q = resultant velocity in the relative (rotating) frame of reference
R = radius ratio (r/r_t)
r_m = mean radius
r, θ, z = radial, tangential, and axial coordinates, respectively ($z=0$ at trailing edge)
S = blade spacing
s, n, r = streamwise, normal, and radial coordinates ($s=0$ at trailing edge, $n=0$ at the wake center)
U, V, W = radial, tangential, and axial velocities (mean) in rotating coordinate system (U is positive in radial outward direction)
U_n, U_r, U_s = relative mean velocities in the normal, radial, and streamwise directions, respectively
u_n', u_r', u_s' = fluctuating components of relative velocities in the normal, radial, and streamwise directions, respectively
u', v', w' = fluctuating component of radial, tangential, and axial velocities
w = defect in axial mean velocities
$(V_\theta)_{abs}$ = absolute tangential velocity
$(\Delta v)_m$ = absolute tangential increment across the wake (difference between the maximum and minimum values)
Y = tangential distance from the wake centerline nondimensionalized by semiblade spacing ($2r\theta/S$, $\theta=0$ at wake centerline, and Y is negative on the suction side and positive on the pressure side of the wake)
Z = axial distance from rotor blade trailing edge nondimensionalized by chord length of rotor blade (C)
δ = wake width $2(L_p+L_s)/S$
Ω = angular velocity of the rotor
ψ = mass averaged pressure rise coefficient
ρ = density
ϕ = flow coefficient ($W_1/\Omega r_m$)
$\tau_r, \tau_z, \tau_\theta$ = normalized turbulence intensities in the radial, axial, and tangential directions, respectively ($\sqrt{u'^2}/W_0$, $\sqrt{w'^2}/W_0$, $\sqrt{v'^2}/W_0$)
i = incidence
τ_{sn}, τ_{rn} = streamwise and radial stresses, respectively ($-\overline{u_s'u_n'}/Q_0^2$, $-\overline{u_r'u_n'}/Q_0^2$)

Subscripts

c = at the wake centerline
m = maximum value in wake
0 = freestream/wake edge value
t = at the tip
∞ = inlet value at midradius
$1,2$ = inlet and outlet of rotor, respectively
abs = absolute
P, S = pressure and suction side, respectively

Presented as Paper 81-0193 at the AIAA 20th Aerospace Sciences Meeting, Orlando, Fla., Jan 11-14, 1982; submitted Jan. 13, 1982; revision received June 28, 1982.

*Director of Computational Fluid Dynamics Studies and Professor of Aerospace Engineering, Department of Aerospace Engineering. Fellow AIAA.

†Graduate Assistant, Department of Aerospace Engineering. Member AIAA.

‡Presently Development Engineer, Avco Lycoming Division, Stratford, Connecticut.

Introduction

THE rotor wake is a major source of unsteadiness, noise, and aerodynamic inefficiency in turbomachinery. Hence, considerable effort has been made in recent years to understand their nature and decay characteristics.[1-3] Most of the data and correlation presently available are valid in regions away from the end walls.

The flow in the annulus wall and hub wall regions at the exit of a turbomachinery rotor develop in the presence of two interacting shear layers; the wakes generated by the rotor blades, and the annulus wall and the hub wall boundary layers, all of which are turbulent and three dimensional in nature. The flow is further complicated by the presence of the secondary flow in these regions. The wake development in the tip region of a compressor rotor at the design condition was reported in Ref. 4.

It is the objective of this paper to study the effects of both the blade loading and the rotation on the wake development in the hub wall and the annulus wall regions. It is known that the rotation induced centrifugal and coriolis forces generate spanwise flows inside the blade boundary layers, the magnitude of which depends on the angular velocity and the blade loading. The effect of rotation and the blade loading on the wake development in the midspan regions was reported in Ref. 5. The data taken from the same rotor in the annulus wall and hub wall regions are presented and interpreted in this paper.

Facility and Measurement Program

Measurements reported in this paper were carried out using the Axial Flow Fan Research Facility (AFRF) at the Applied Research Laboratory. The facility and the rotor are described in detail in Refs. 5 and 6 and will not be repeated here.

The rotor alone (no IGV or stator) was operated at the design point at two different rotational speeds, $N=1753$ and 1010 rpm. Identical inlet incidence ($i=3$ deg at midradius) at two differing rotational speeds was achieved by means of an auxiliary fan at the exit of the facility. These sets of measurements provide the wake data at two differing speeds (1753, 1010 rpm) at the same blade loading ($\phi=0.6$) and two different blade loadings ($\phi=0.6$ and 0.7). The data near the midspan region, $R=0.628$, 0.72, 0.813, were reported and interpreted in Ref. 5. The data at the hub wall region ($R=0.488$, 0.534) and the annulus wall regions ($R=0.91$, 0.953) are presented and interpreted in this paper.

The radial variation of the axial and the tangential velocity at the inlet and the exit of the rotor were measured by Pierzga[6] using a five hole pitot probe. These are plotted in Fig. 1. As mentioned earlier, the facility was operated at $\phi=0.6$ and 0.7. Since no exit or inlet data are available for $\phi=0.7$, the data at $\phi=0.72$ is shown. The radii at which the wake data is reported in this paper are also shown in Fig. 1. Two of these stations are inside the hub wall boundary layer and two inside the annulus wall boundary layer.

Rotor Wakes Near the Hub Wall

The hot-wire data near the hub wall regions at $R=0.488$ and 0.534 and at various axial locations are presented in this section. The mean velocity data, unless otherwise stated, are in the absolute frame of reference in axial (z), tangential (θ), and radial coordinate (r) system. The tangential distance (Y) is normalized by the semiblade spacing. Hence $Y=0$ represents the wake center, $Y=\pm 1.0$ represents the midpassage. All velocities are normalized by the corresponding freestream axial velocity. The profiles at $R=0.488$ consist of only the near-wake data for the effect of loading, while the profiles at $R=0.534$ include both the near- and far-wake data at all operating conditions. Since all the data presented in this paper are nondimensionalized by W_0, their values at $Z=0.166$ are given in Table 1. Variation of this quantity downstream is found to be negligible. The turbulence intensities are normalized by the freestream axial velocity. The turbulent shear stresses of practical interest are the streamwise stress, $-\rho u_s' u_n'$, and radial stress, $-\rho u_n' u_r'$, in the relative coordinate system. These were derived from the hot-wire data transformed into streamwise (s), normal (n), and radial (r) coordinate system. The stresses are normalized by ρQ_0^2, where Q_0 is the resultant relative velocity in the freestream.

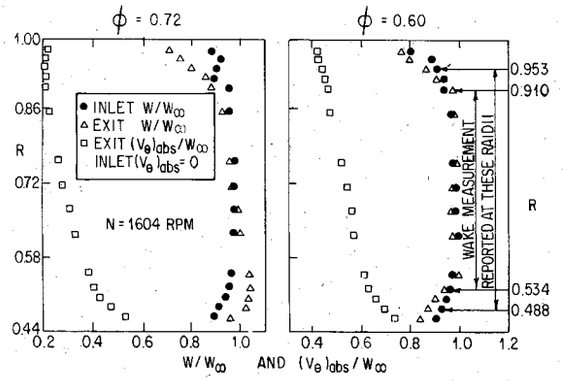

Fig. 1 Radial variation of axial and tangential velocities at inlet and exit of the rotor at $\phi=0.6$ and $\phi=0.7$ (Ref. 6).

Table 1 Freestream axial velocity (W_0) at $Z=0.166$

R	0.488	0.534	0.91[a]	0.953
W_0, ms 1753 rpm	22.9	23.3	22.73	14.8
W_0, ms 1010 rpm	--	17.3	--	10.77
W_0, ms 1499 rpm	23.1	24.5	18.7	15.77

[a] Values at $Z=0.252$.

Mean Velocity Profiles

The axial, radial, and absolute tangential velocity profiles at $R=0.488$ inside the hub wall boundary layer is shown in Fig. 2. Only two axial stations ($Z=0.042$, 0.167) are shown for brevity. An increase in the blade loading tends to increase the axial velocity defect at $Z=0.042$. This is consistent with the measurement of the wake near the midspan,[5] but this trend is reversed at $Z=0.167$, where the axial velocity defect is smaller at the higher blade loading.

The presence of the secondary flow is evident from the tangential (absolute) and radial velocity profiles shown in Fig. 2 for $R=0.488$. At both operating conditions, $(V_\theta)_{abs}$ distribution indicates overturning on the suction side and underturning on the pressure side, with almost linear distribution inside the wake. The distribution of $(V_\theta)_{abs}$ shows that the secondary flow is more severe at lower loading (as evidenced by the larger difference in $V_{\theta_{abs}}$ between the two sides), even though the absolute tangential velocity is lower in this case. One possible reason for such a behavior is the radial transport of angular momentum caused by the radial velocity, which is higher at higher loading (Fig. 2). It is also evident that the tangential velocity distribution is substantially different from those observed at the midradius,[5] where a conventional wake profile is observed with the highest $V_{\theta_{abs}}$ occurring at the wake center.

The radial velocity profile at $R=0.488$, plotted in Fig. 2, shows substantial differences between the two loadings. It is inward for $\phi=0.7$ and outward near the suction surface for $\phi=0.6$. Since the radial velocities are small, their absolute magnitudes are very sensitive to the accuracy with which the hot-wire sensor angles can be measured. Hence, if the interpretation is based on the qualitative nature of the velocity profile, the dominance of the secondary flow, as well as the radial flow in the blade boundary layer, is evident from Fig. 2. The secondary flow (in a rotor alone configuration) is inward near the pressure surface and outward near the suction surface, while the radial flow due to rotation is outward near both surfaces. Hence, these effects are additive on the suction side and subtractive on the pressure side. This trend is evident for $\phi=0.6$ at both axial locations. The radial velocity at $\phi=0.7$ shows the opposite effect; namely, larger inward flow

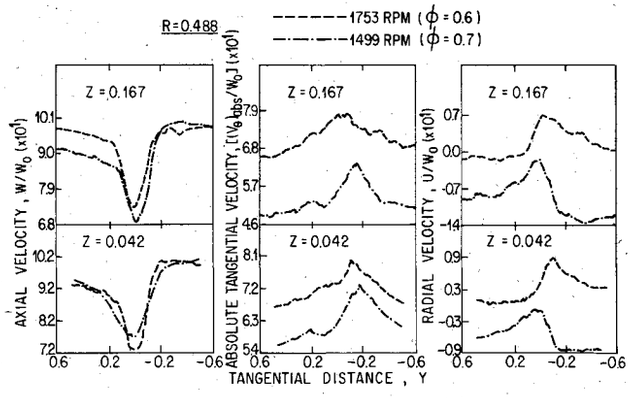

Fig. 2 Axial, tangential, and radial velocity profiles at $R=0.488$.

on the suction side. Nevertheless, the distribution of U is similar to that observed in a vortex system. Hence, the type of radial velocity distribution measured near the hub at $\phi = 0.7$ seems to indicate a flow dominated by the secondary flow and a vortex system rather than the rotation.

The axial, radial, and absolute tangential velocity profiles across the wake at $R = 0.534$, which is still inside the hub wall boundary layer but closer to the outer edge, is shown in Fig. 3. The data set includes the near and far wake, as well as the loading and rotation effects. The effect of loading on the axial velocities profile is similar to those observed at $R = 0.488$. The lowest loading has the least defect in the axial velocity. This trend is similar to that observed by Shaw and Balombin[3] at 80% span from the tip in their high-speed compressor. The defect is nearly the same at both loading (1753 and 1499 rpm) at $Z = 0.167$. The effect of increase in the speed (compare the plot for $\phi = 0.6$, 1010, and 1753 rpm) is to decrease the wake defect in the near wake, with essentially no differences far downstream. This trend is very similar to that reported in Ref. 5 at midspan of the same rotor.

The distribution of absolute tangential velocity at $R = 0.534$ shows a trend similar to that observed at $R = 0.488$, but dissimilar to the measurements at the midspan.[5] The secondary flow effects persist, even at this location, with overturning on the suction side and underturning on the pressure side. A vortex rather than a wake type of distribution is observed at this radius. The secondary flow/vortex seems to decay rapidly downstream, especially for the higher speeds. This is caused by the higher radial velocity and the associated flow transport. The strength of the secondary flow appears to be about the same at both speeds at the same loading (1753, 1010 rpm), even though the absolute levels of tangential velocities are higher at the higher speed. The loading effect is similar to that observed at $R = 0.488$.

The radial velocity distribution at $R = 0.534$ shows considerable differences with the change in rotational speed and the blade loading. The radial velocities are lowest at the lower loading and are mostly outward, unlike the corresponding data at $R = 0.488$. The distribution inside the wake indicates the presence of a trailing vortex due to a change in circulation along the span. This vortex is in the same direction as that observed at $R = 0.488$ (see Fig. 2). The change in the radial velocity due to the change in rotational speed is much more dramatic. At 1753 rpm, the cumulative effect of the secondary flow (or the trailing vortex) and the outward movement of the flows inside the blade boundary layer is evident on the suction side, where the radial outward velocities are as high as 20% of the axial velocity. The subtractive effect of the two is evident on the pressure side. Radial velocities are generally high even in the freestream. The radial velocity in the freestream is inward for the lower rpm case. The effect of the secondary flow at this radial location is thus evident. One of the reasons for the drastic change in the magnitude of the radial velocity may be due to the change in the entry boundary layer. In the higher rpm case the skewness of the entry boundary layer is much larger than those at the lower rpm case (1010 rpm). Thus, the secondary flow (which depends on the entry vorticity) is altered in the two cases under consideration.

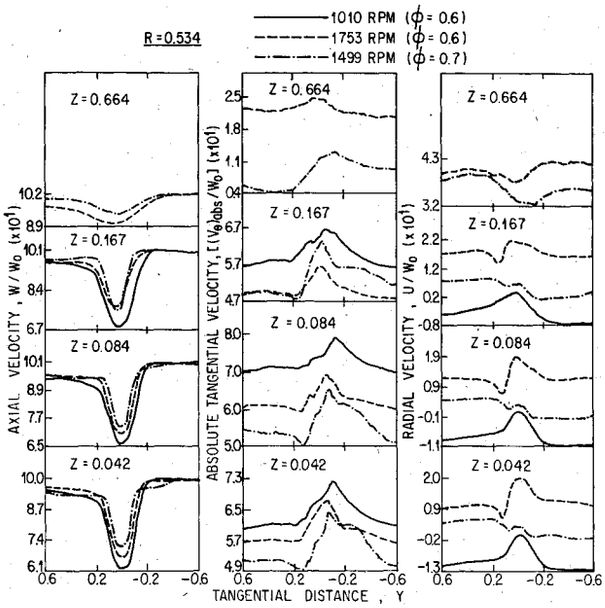

Fig. 3 Axial, tangential, and radial velocity profiles at $R = 0.534$.

Variation of Wake Parameters

The wake parameters of practical significance are axial velocity defect at the centerline (w_c), absolute tangential velocity increment $(\Delta v)_m$ across the wake, maximum difference in radial velocity across the wake $(U_p - U_s)_m$, and the wake width (δ). These are shown plotted in Figs. 4 and 5 and are compared with values at other radii.

It is clear from Fig. 4 that the axial velocity defect is maximum at the lower speed and minimum at the lower loading at $R = 0.534$. The rate of decay of w_c is nearly the same in the near wake for all operating conditions. Comparing this with the values of w_c at the midradius (shown in Fig. 4), it is clear that w_c generally is higher near the hub region. The data also indicate a slower decay of the near wake

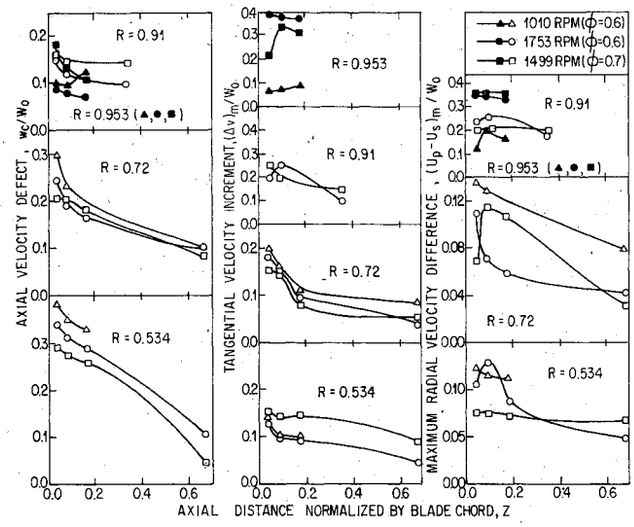

Fig. 4 Decay of maximum axial velocity defect, maximum absolute tangential increment, and maximum radial velocity difference at various radii.

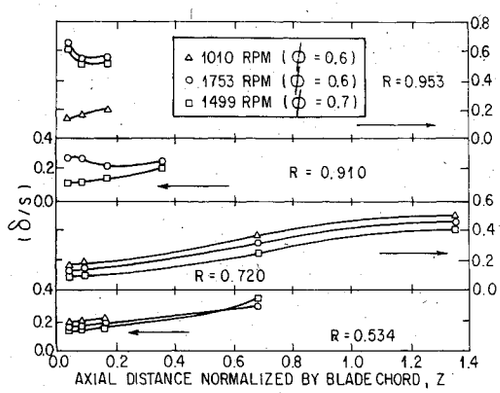

Fig. 5 Axial variation of wake width at various radii.

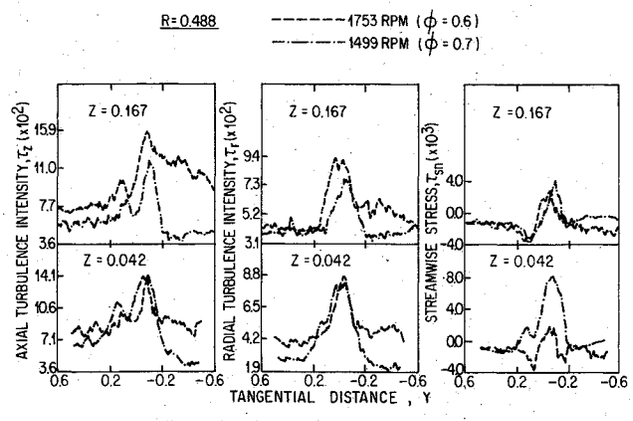

Fig. 6 Axial and radial intensity profiles and streamwise stress distribution at $R=0.488$.

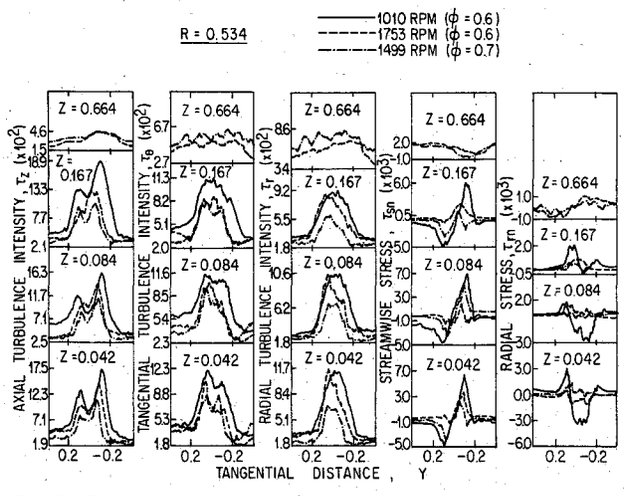

Fig. 7 Turbulence intensity and shear stress profiles at $R=0.534$.

in the hub region as compared to the decay of the near wake at the midradius.

The decay of the increment in absolute tangential velocity $(\Delta v)_m$ at $R=0.534$ shows a peculiar trend. As mentioned earlier, the behavior of the absolute tangential velocity mainly is controlled by the secondary flow phenomena at this region. The lower loading ($\phi=0.7$) has the maximum value of $(\Delta v)_m$, and the decay is also slower. The change of speed at $\phi=0.6$ seems to have very little effect on the value of $(\Delta v)_m$ at $\phi=0.6$, a confirmation of the fact that the parameter $(\Delta v)_m$ is controlled by the hub wall boundary layer and the secondary flow inside this layer as opposed to the wake-dominated phenomena. The increment $(\Delta v)_m$ at $R=0.72$ is caused primarily by the rotor wake. This decays very rapidly as shown in Fig. 4.

The maximum radial velocity difference across the wake at $R=0.534$ is minimum at lower loading. They generally are higher at lower rotational speeds. One possible reason for this is the fact that the radial velocity difference in this case mainly is controlled by secondary flow, which should be nearly independent of the rotational speed. The radial velocity difference at $R=0.534$ is lower than their values at the midradius, where the rotation effects influence the wake parameters.

The wake width δ (based on axial velocity profile) at $R=0.534$ is shown plotted in Fig. 5. The wake width is generally of the same order of magnitude as those at $R=0.72$ and follows the same trend. The wake width is higher at the higher loading at the lower speed. The wake width in the far wake ($Z=0.667$) is higher near the hub.

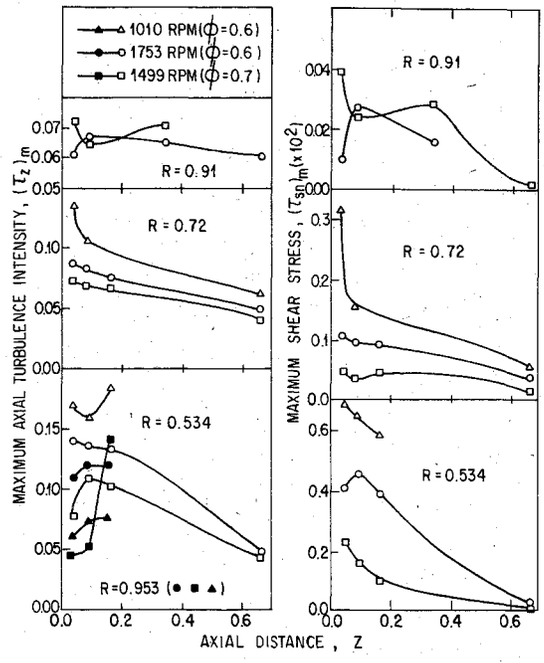

Fig. 8 Decay of maximum axial, tangential, and radial turbulence intensities at various radii.

Turbulence Properties

The distribution of the axial, tangential, and radial turbulence intensities as well as the streamwise stress at $R=0.488$ is shown in Fig. 6. The turbulence intensities are identical in both the rotating and stationary coordinate system.

The axial and radial turbulence intensities at $R=0.488$ are higher than those measured at the midradius,[5] with peak values at the wake center ranging from 14 to 16%. The values of τ_z generally are higher at the higher loading. The freestream intensities are also higher. The radial component of intensity (τ_r) is much lower than the axial component (τ_z), an indication that the effect of rotation on the turbulence structure is small in this region.[7] The freestream value of τ_r is also smaller than τ_z in both cases. The streamwise stress (τ_{sn}) is higher at lower loading in the near wake. This behavior is somewhat strange and contrary to expectations; but, far downstream the values τ_{sn} are nearly identical for both operating conditions.

All three components of turbulence intensities and the two components of shear stresses (τ_{sn}, τ_{rn}) at $R=0.534$ for all the operating conditions are plotted in Fig. 7. All three components of intensities are highest at the lower rotational speed ($\phi=0.6$) and lower at lower loading ($\phi=0.7$). The dip in the turbulence intensities, normally present in the near wake, is observed only for the axial velocity component. The peak intensities are higher than those observed at $R=0.488$, but the freestream intensities are much lower. This is expected since $R=0.534$ is in the outer layer of the hub wall boundary layer. The radial and tangential components of turbulent intensities are nearly the same, while the axial components are generally higher at most locations.

The blade-to-blade distribution of streamwise and radial components of stresses, τ_{sn} and τ_{rn}, at $R=0.534$, shown in Fig. 7, indicate that these decay rapidly to negligibly small values in the far downstream location. The peak stresses occur away from the wake centerline and are of the opposite sign on either side of the wake. The streamwise components of stress are generally higher than the radial components. The stresses are higher at lower rotational speeds and higher loading. This is consistent with the mean velocity distribution shown in Fig. 3, where the axial velocity gradient is maximum at 1010 rpm near the wake center.

The decay of the maximum axial turbulence intensity (τ_z) and maximum streamwise stress (τ_{sn}) at $R=0.534$ is shown in Fig. 8. The trend is somewhat confusing, as this region is dominated by the rotor wake, hub wall boundary layer, and secondary flow. The values of $(\tau_z)_m$ are higher at the lower rotational speed ($\phi=0.6$) and lower for the lower loading case ($\phi=0.7$). The values of $(\tau_z)_m$ increase in the near wake at 1010 rpm ($\phi=0.6$) and 1499 rpm ($\phi=0.7$), a trend not observed at $R=0.72$. This seems to indicate the development of the secondary flow/vortex, which has a tendency to amplify the turbulence intensities. Further downstream ($z>0.167$) the intensities decay at about the same rate as $R=0.72$. The maximum value of the streamwise stresses $(\tau_{sn})_m$ at $R=0.534$ is generally much higher than those observed at $R=0.72$, with the highest values observed at a lower rotational speed. The lower loading has the lowest value of $(\tau_{sn})_m$.

Rotor Wakes Near the Annulus Wall

Measurements near the annulus wall, at $R=0.91$ and at $R=0.953$ (Fig. 1), and at various axial locations are presented in this section. The data include the effects of rotation and the blade loading. The flow in the annulus wall region is quite different from the flow in the hub wall region. Unlike the rotating hub, the annulus wall is stationary resulting in a relative motion between the blades and the annulus wall. The tip clearance between the blade and the wall also has a considerable influence on the flow in the region. Further, the radial migration of flow toward the tip results in an accumulation of low momentum fluid in the region. These effects considerably alter the characteristics of flow in the region and tend to dominate the simple wake flow found around the midradius of the blade.[5]

Mean Velocity Profiles

The axial, radial, and absolute tangential velocity profiles at $R=0.91$ at three axial locations are shown in Fig. 9. Only the effects of loading are shown at this radial location. Unlike the data near the hub wall and the midradius, the axial velocity defect at the lower loading is higher than that at the higher loading. One probable reason for this is the change in the annulus wall boundary-layer development due to a larger migration of low momentum fluid in the region at the higher loading which causes the wake to decay much more rapidly than at the lower loading. This is also evident in Fig. 4 where the axial variation of the axial velocity defect has been plotted. The distribution of the absolute tangential velocity is very similar to those observed at the midradius[5] and is unlike the distribution near the hub region. The peak values occur at the center of the wake, which seem to indicate the absence of secondary flow in the region. The increment $(\Delta v)_m$ and the decay rate are nearly the same at both operating conditions, even though $(V_\theta)_{abs}$ is higher at the higher loading, as would be expected. The magnitude of the radial velocities are substantially higher than their values at the midradius or the hub region. The distribution of radial velocity at $R=0.91$ is also substantially different from other radii. The radial velocities are minimum at the wake center and increase gradually to large values toward the midpassage. Pierzga[6] has also reported large radial outward velocities (passage averaged) in this region. His data were acquired in the same facility using a five hole probe at the exit. One possible cause for this is the presence of a tip vortex and the entrainment associated with its development. This probably accounts for the large radial velocity at all locations of the passage at this radius.

The axial, radial, and absolute tangential velocity profiles at $R=0.953$ at three axial locations are shown in Fig. 10. The effects of both the loading and the rotation are presented at this radial station. It is clear from these profiles that the characteristics of this flow are quite different from those away from the wall regions. The presence of a substantial low momentum fluid that accumulates in this region from the radial migration of the flow is evident in addition to the presence of the blade wake. This accumulated fluid interacts and sometimes dominates the blade wake. This is clear in the axial velocity profiles at $Z=0.042$. At 1753 rpm ($\phi=0.6$), the blade wake is completely dominated by this body of fluid. A blade wake is more visible at 1499 rpm ($\phi=0.7$) and is the dominant flow at 1010 rpm. This would indicate that the radial migration of low momentum fluid and the blade boundary-layer growth is influenced by the rotational speed and the blade loading. The flow characteristics deteriorate rapidly as the rotational speed is increased. Again, as at $R=0.91$, the axial velocity defect is higher at the lower loading, which is opposite to the trend seen at $R=0.72$. The absolute tangential velocity profiles at 1753 and 1499 rpm show a larger effect of the secondary flowfield which was absent at $R=0.91$. The profiles of $(V_\theta)_{abs}$ differ substantially from those observed at $R=0.72$ and 0.91, but follows the trend seen near the hub. The peaks occur on either side of the wake. This evidently is caused by the secondary flow/vortex or tip vortex. This effect is slightly greater at 1753 rpm as seen at $Z=0.042$. The profiles at 1010 rpm show peculiar characteristics and almost no wake or secondary flow at all. This may be due to the data processing procedure, the wake being washed out by the averaging procedure due to unsteadiness in the flow. The radial velocity in the freestream is large, similar to that at $R=0.91$. An inward velocity is observed in the wake at 1010 rpm. The radial velocities in the wakes as well as the freestream are higher than those measured at $R=0.91$. The comments made with regard to the radial velocity distribution at $R=0.91$ are valid for this case also. The radial velocities are higher at higher rpm and lowest at 1010 rpm. This seems to indicate the predominant influence of the rotation and the presence of the tip vortex in this region.

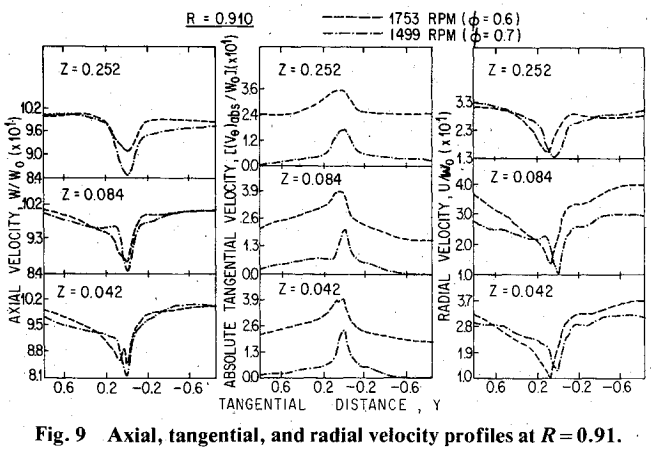

Fig. 9 Axial, tangential, and radial velocity profiles at $R=0.91$.

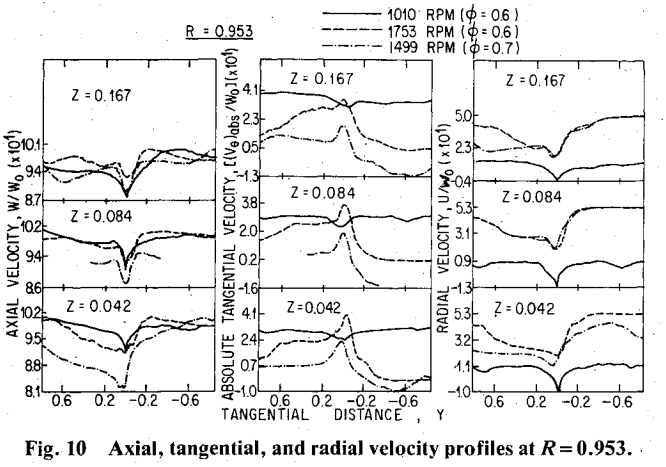

Fig. 10 Axial, tangential, and radial velocity profiles at $R=0.953$.

Variation of Wake Parameters

The important wake parameters, the axial velocity defect (w_c), the tangential velocity increment $(\Delta v)_m$ across the wake, the maximum difference in the radial velocity across the wake $(U_p - U_s)_m$, and the wake width (δ), at $R = 0.91$ and $R = 0.953$ are plotted in Figs. 4 and 5 and compared with the values at the other radii. At $R = 0.91$, the axial velocity defect is higher at the lower loading than at the higher loading. This is opposite to the trend at the lower radii. The decay of the axial velocity defect is faster at the higher loading and probably accounts for the reversal of the trend. At $R = 0.953$, the axial velocity defect is highest at the lower loading similar to that at $R = 0.91$ and opposite to the trend at $R = 0.72$. The defect is higher at the lower rotation (1010 rpm) than at the higher rotation (1735) for the same loading. This trend is similar to that at the lower radii ($R = 0.72$).

The trends in the tangential velocity increment $(\Delta v)_m$ at R = 0.91 and $R = 0.953$ are similar to those at the lower radii. An increase and a subsequent decay in these distributions are probably due to the large mixing of the flow in the region. The decay of $(\Delta v)_m$ at the higher loading is faster than that at the lower loading at $R = 0.91$, similar to that at $R = 0.72$ and $R = 0.534$. The decay rates are not substantially different at $R = 0.953$. The $(\Delta v)_m$ distribution at the lower rotation is uncertain, as mentioned in the previous section.

The maximum radial velocity difference for the two different loadings at $R = 0.91$ and 0.953 are not substantially different. The maximum radial velocity difference in this region is probably controlled by the development of the tip vortex. The lowest rotation (1010 rpm) indicates the minimum radial velocity difference, a trend opposite to that at the lower radii and indicative of the different controlling factor for the radial velocity in this region.

The axial variation of the wake width is shown in Fig. 5. The wake width in this region is controlled by both the loading and the rotation. A higher loading results in a thicker boundary layer at the trailing edge and a larger wake width. The wake width is also indicative of the accumulation of low momentum fluid in the region from the radial transport of this fluid. The wake width at $R = 0.91$ at the higher loading is substantially higher than at the lower loading. At $R = 0.953$ the higher rotation has a much larger wake width than at the lower rotation, again indicating the larger accumulation of low momentum fluid in the tip region as the rotational speed is increased. The slight decrease and subsequent increase in the wake width at the two different loadings is probably due to the intense mixing of the flow in the tip region.

Turbulence Properties

The distribution of all the components of turbulence intensities and the shear stresses at $R = 0.91$ are plotted in Fig. 11. The turbulence intensities are lower than those observed near the midradius[5] and the hub regions (Figs. 6 and 7). The intensities generally are higher at higher loading. The radial component of turbulence intensities (both in the wake and in the freestream) are higher (about 25-30%) than the corresponding axial and tangential components. The effect of rotation, which has a tendency to amplify the radial component of intensities and attenuate the other components[7] is clearly evident here. The major difference in loading effect occurs in regions away from the wake. The streamwise shear stresses in the wake are generally higher for the lower loading, this trend is reversed away from the wake. Perhaps the most important conclusion in regard to the shear stress is the fact that both the radial and the streamwise stresses are of the same order of magnitude, even though the radial velocities and their gradients are smaller than the corresponding values in the streamwise direction. This again is the effect of rotation on the turbulence structure analyzed in Ref. 7.

The axial, radial, and tangential components of turbulence intensities at $R = 0.953$ are shown in Fig. 12. It is evident that this region has the most complex and least organized motion, both in terms of the magnitude and the distribution of intensities. The intensities are higher throughout the passage, an effect caused by large viscous effects and mixing in the entire blade passage. Near the trailing edge, the axial turbulence intensities are highest at higher speeds and higher loading with substantially lower values at other operating conditions. This evidently is caused by the intense flow mixing due to higher

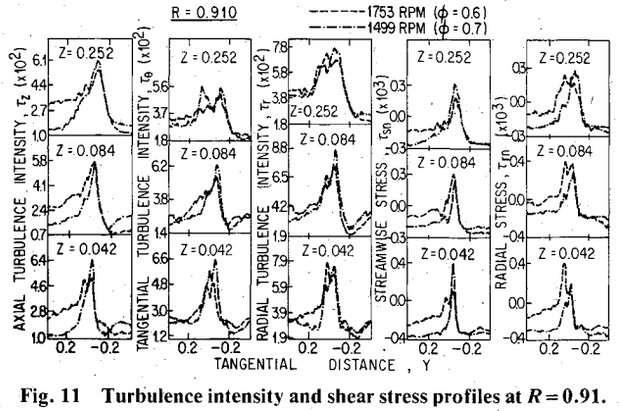

Fig. 11 Turbulence intensity and shear stress profiles at $R = 0.91$.

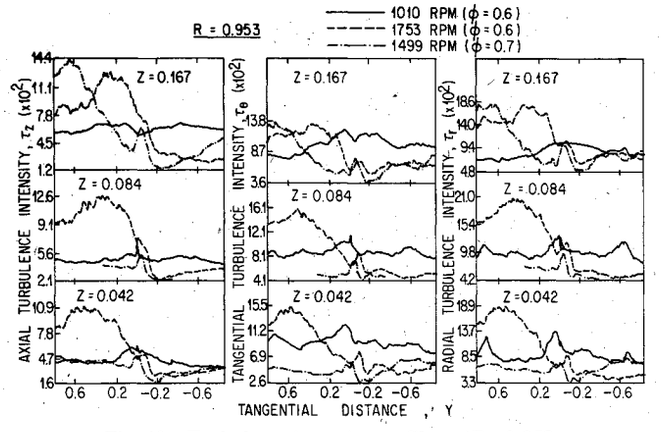

Fig. 12 Turbulence intensity profiles at $R = 0.953$.

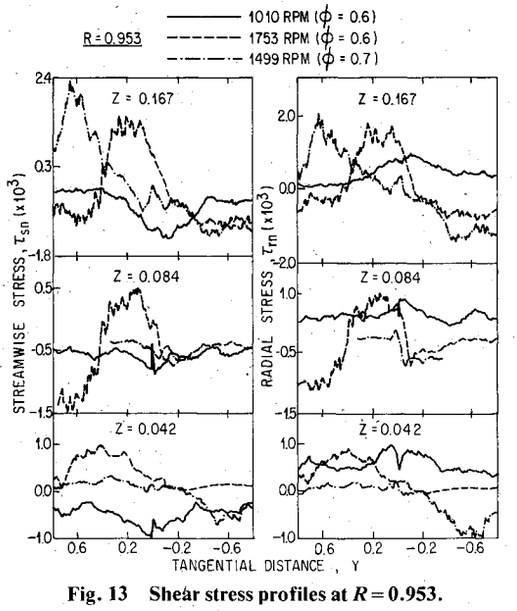

Fig. 13 Shear stress profiles at $R = 0.953$.

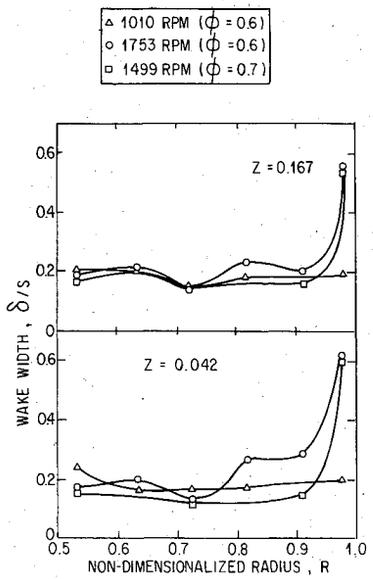

Fig. 14 Radial variation of wake width at various operating conditions.

radial velocities at 1753 rpm (Fig. 10). While this effect persists even up to $Z=0.167$, the axial intensities get amplified beyond $Z=0.084$ for the lower loading case (1499 rpm). This may have been caused by the development of a tip vortex in this region. The lower rpm has the lowest intensities. The axial component of intensity is the lowest at all locations followed by the tangential and the radial component. This situation is quite different from those observed at the midradius[5] and the hub regions (Figs. 6 and 7). The effect of rotation is felt in the increased radial turbulence intensities, while the development and decay of the vortex would influence both the tangential and radial components. This seems to be the most plausible explanation.

The distribution of the radial and the streamwise components of shear stresses at $R=0.953$ is shown in Fig. 13. The comments made in regard to the turbulence intensities are valid here also. Both the stresses increase in magnitude downstream, caused probably by the development and decay of a vortex. The radial component of shear stresses are generally of the same order of magnitude as the streamwise component. The stresses are high throughout the flowfield, but the peak values (due to wake) generally are lower than those observed at $R=0.91$ and 0.72.

The decay of the maximum axial turbulence intensity and the streamwise stress at various operating conditions are shown in Fig. 8. As explained earlier, values of $(\tau_z)_m$ at $R=0.91$ are lowest and the decay is slowest of all the radii, especially those measured at $R=0.534$ and 0.953. The plot of τ_{z_m} at $R=0.953$ shows a trend similar to those observed at $R=0.534$, namely an increase in $(\tau_z)_m$ in the near wake. The decay seems to be much less rapid than any other radii. The plot of maximum streamwise stress for $R=0.91$ indicates that they are much lower than all other radii for which the measurements are available.

Radial Variation of the Wake Width

The radial variation of the wake width is shown in Fig. 14. This plot dramatically shows the effect of rotation on the radial migration of low momentum fluid. As the rotation speed is increased a larger amount of fluid is thrown out from the hub to the tip. Thus, the wake width is lower at the higher rotation near the hub and up to the midradius but rapidly increases toward the tip and is substantially larger there. Even at the lower loading (1499 rpm), the wake width at the tip is substantially larger than at the lower rotation speed (1010 rpm).

Conclusions

Some of the important conclusions that can be drawn from the investigations reported in this paper are as follows.

1) The rotor wake near the hub and the annulus walls are substantially different from those observed at other radii. The blade rotation has a dominant influence on the wake near the tip. The change of rotational speed has much less influence on the flow near the hub.

2) The nature of spanwise (radial) flow and the overturning and underturning of the flow observed in the wake near the hub indicate the dominance of secondary flow in this region. Unlike the conventional wake, the peak tangential velocities (absolute) occur away from the wake center.

3) The wake defect is minimum at lower blade loading and maximum at lower rotational speed (at the same blade loading) near the hub region. The velocity defects near the hub are much higher than the defects at all other radii.

4) The radial velocities are higher at higher rotational speeds and lower at lower loading in the hub region.

5) The wake width and its growth rate near the hub are nearly the same as those observed near the midradius.

6) The turbulence intensitites are higher at the lower rotational speed (for the same loading) and lower for the lower loading case near the hub region. The turbulent shear stresses behave in a like manner.

7) The axial velocity defect reverses the trend in the tip region, the defect is larger at the lower loading than at the higher loading. The defect is smaller at higher rotation than at lower rotation, a trend similar to that at lower radii.

8) The secondary velocity field has a large influence on the absolute tangential velocity profile and alters it considerably from that at the midradius location.

9) The radial velocity profile is substantially different in the tip region from that at the lower radii and is probably due to the development of the tip vortex.

10) A dominant flow phenomenon in the tip region is the accumulation of low momentum fluid in the region caused by the radial migration of this fluid toward the tip. This body of fluid alters and dominates the conventional wake flow found at the midradius.

11) The migration of low momentum fluid toward the tip is largely controlled by the rotation speed and is reflected in a large increase in the wake width in the tip region as the rotational speed is increased.

12) The wake width is smaller at a lower loading at all radial locations. The wake width is high near the tip for all operating conditions, except the lowest rotation.

13) Even though an increase in the rotation speed seems to improve the flow in the hub region and up to the midradius in terms of a smaller wake width and lower boundary-layer growth on the blade, it rapidly deteriorates the flow in the tip region.

Acknowledgments

This work was supported by NASA through Grant NSG 3012, with L. Shaw as the technical monitor. The experimental work was carried out at the Applied Research Laboratory in their Axial Flow Research Fan Facility. Assistance by J. Rishell and W. Nuss is gratefully acknowledged.

References

[1] Reynolds, B. and Lakshminarayana, B., "Characteristics of Lightly Loaded Fan Rotor Blade Wakes," NASA CR 3188, Oct. 1979.

[2]Dring, R. P., Joslyn, H. D., and Hardin, L. W., "An Investigation of Axial Compressor Rotor Aerodynamics," *Journal of Engineering for Power,* Vol. 104, Jan. 1982, pp. 84-96.

[3]Shaw, L. M. and Balombin, J. R., "Rotor Wake Characteristics Relevant to Stator-Rotor Interaction," NASA TM82703, Oct. 1981 (also AIAA Paper 81-2031).

[4]Davino, R. M. and Lakshminarayana, B., "Characteristics of Mean Velocity in the Tip Region of Turbomachinery Rotor Exit," *AIAA Journal,* Vol. 20, April 1982, pp. 528-535.

[5]Lakshminarayana, B., Govindan, T. R., and Reynolds, B., "Effects of Rotation and Blade Incidence on the Properties of Turbomachinery Rotor Wake," *AIAA Journal,* Vol. 20, Feb. 1982, p. 245.

[6]Pierzga, M. J., "Experimental Verification of the Streamline Curvature Numerical Analysis Method Applied to the Flow Through an Axial Flow Fan," M.S. Thesis, Dept. of Aerospace Engineering, The Pennsylvania State University, 1981 (also, ARL TM 80-181, May 1980).

[7]Lakshminarayana, B. and Reynolds, B., "Turbulence Characteristics in the Near Wake of a Compressor Rotor Blade," *AIAA Journal,* Vol. 18, Nov. 1980, pp. 1354-1362.